Excitation of low-energy H atoms in H + Ne collisions

B. Van Zyl, M. W. Gealy, and H. Neumann
Department of Physics, University of Denver, Denver, Colorado 80208
(Received 1 December 1984)

Excitation of 0.05—2.5-keV H atoms in H+Ne collisions has been examined by measuring the absolute emission cross sections for Balmer-α, Balmer-β, and Lyman-α radiations resulting from the collisions. Lyman-α emission was also observed when an electric field was applied in the interaction region to investigate excitation of H atoms to the (metastable) $2s$ state. The radiation polarization for each of the above emissions was measured. A new method for absolute calibration of the Lyman-α detector is described, and Lyman-α emission cross sections for $H^+ + Ar$ and $e^- + H_2$ collisions are compared with previous results, the latter reaction giving a significantly smaller cross section than generally accepted. The peculiar behavior of the H+Ne interaction indicated by the measurements is discussed.

I. INTRODUCTION

In earlier publications,[1-3] the absolute emission cross sections and radiation polarizations for Balmer-α (H_α) and Balmer-β (H_β) emissions resulting from low-energy H collisions with Ar, He, H_2, N_2, and O_2 targets were reported for laboratory H energies between about 0.05 and 2.5 keV. This paper begins with a report in Sec. II of similar measurements for H + Ne collisions. The absolute calibration of the photon detector used for this work has been described earlier,[1] and will not be reviewed here.

However, because this is the first of a series of papers which will report Lyman-α (L_α) emission cross sections for various reactions, the L_α detector and its absolute calibration are described in detail in Secs. III and IV. The cross sections for L_α emission from $H^+ + Ar$ and $e^- + H_2$ collisions measured with this detector calibration are compared with other data in Sec. IV.

The results of the L_α emission cross-section measurements for H + Ne collisions are presented in Sec. V. By analysis of these data and those for H_α and H_β emission presented in Sec. II, the fractions of the total L_α from direct excitation and from cascade population of the $2p$ state were determined.

Section VI describes the observations made of the L_α emission from H + Ne collisions when a 700 V/cm electric field was applied to the interaction region. An analysis of these data resulted in a determination of the cross section for excitation to the (metastable) $2s$ state of H in the collisions.

The results of these various measurements are summarized in Sec. VII, where they are compared with results from collisions of H with other target species. An approximate determination of the polarization of L_α emission from the electric-field-induced decay of the $2s$ state of H is also presented there.

The techniques used in these experiments to generate the H-atom beam and to measure the target-cell pressure have been described in earlier papers,[1,4,5] and will not be discussed here. All photon signals were measured as a function of target-cell pressure, and the normalized photon signals (i.e., the actual signals divided by the pressure) were extrapolated to zero pressure to eliminate the influence of second-collision processes occurring in the target cell.

For all reactions investigated, the polarizations of the emitted radiations were measured. The polarizations are defined by $P=(I_{\|}-I_{\perp})/(I_{\|}+I_{\perp})$, where $I_{\|}$ and $I_{\perp}$ are the emission intensities at 90° to the H-beam axis with their electric vectors parallel and perpendicular to the H-beam axis, respectively. These data were used to obtain total cross sections Q from the cross sections Q' measured for photon emission at 90° to the beam axis: $Q=Q'(1-P/3)$. In this paper, cross sections labeled Q' will always refer to measured (or calculated) data associated with photon emission at 90° to the H-beam axis.

II. H_α and H_β EMISSION CROSS SECTIONS

The measured total H_α and H_β emission cross sections, $Q_{em}(H_\alpha)$ and $Q_{em}(H_\beta)$, are plotted in Fig. 1 versus laboratory H-atom energy (E). For $E>0.2$ keV, the cross sections $Q_{em}(ns\rightarrow 2p)$ and $Q_{em}(np\rightarrow 2s+nd\rightarrow 2p)$ for $n=3$ or 4 identify the divisions of $Q_{em}(H_\alpha)$ or $Q_{em}(H_\beta)$ according to the indicated H-atom transitions causing the emissions. These divisions were determined by measuring the increases in the H_α and H_β signals with increasing distance into the target cell due to the delayed decay of the long-lived ns states of H.[1] (The short-dashed curves labeled $np\rightarrow 2s$ and $nd\rightarrow 2p$ will be discussed in Sec. V.) The polarizations of the total H_α and H_β radiations, used to determine the Q shown from the measured Q', are presented in Fig. 2.

The uncertainties in $Q_{em}(H_\alpha)$ and $Q_{em}(H_\beta)$ are $\pm 13.4\%$ and $\pm 13.7\%$, respectively, for $E\geq 0.1$ keV, increasing to about $\pm 20\%$ at the lowest E. For $E>0.25$ keV, $Q_{em}(3s\rightarrow 2p)$ and $Q_{em}(4s\rightarrow 2p)$ are uncertain by $\pm 13.5\%$ and $\pm 14.3\%$, respectively, while $Q_{em}(3p\rightarrow 2s+3d\rightarrow 2p)$ and $Q_{em}(4p\rightarrow 2s+4d\rightarrow 2p)$ are about twice as

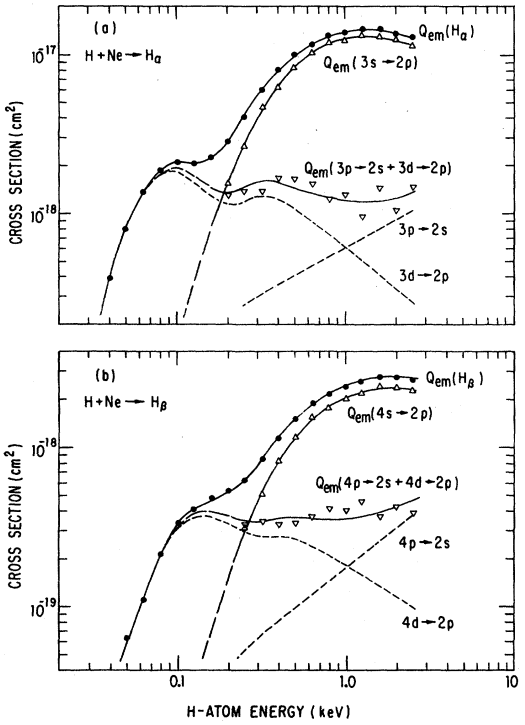

FIG. 1. H_α and H_β emission cross sections for H + Ne collisions.

uncertain. These uncertainties were determined by quadrature combination of all individual uncertainties known to affect the measured data or its analysis, the largest of which is the $\pm 10.2\%$ assigned to the absolute calibration[1] of the photon detector used. Typical uncertainties in the radiation polarizations are flagged in Fig. 2.

The most striking feature of the data in Fig. 1 is clearly the large contributions to the total H_α and H_β emissions made by the $ns \rightarrow 2p$ transitions for $E > 0.32$ keV. For no other target species (including the published results[1-3] for Ar, He, H_2, N_2, and O_2, or the unpublished results[6] for Kr and Xe) has ns-state excitation been so dominant. That most of the H_α and H_β emissions result from $ns \rightarrow 2p$ transitions for $E > 0.32$ keV is consistent with the small radiation polarizations shown in Fig. 2, for $ns \rightarrow 2p$ transitions must give unpolarized radiations (because of the

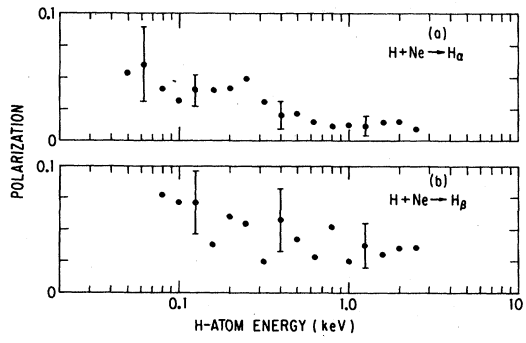

FIG. 2. Polarization of H_α and H_β radiation from H + Ne collisions.

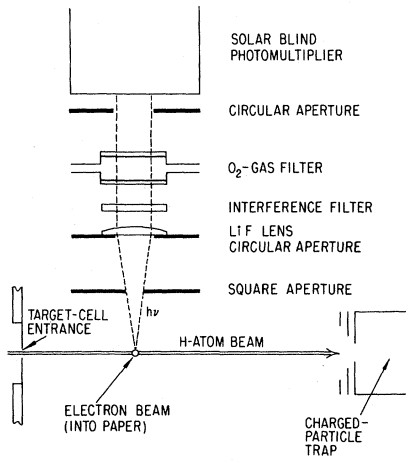

FIG. 3. Photon detector for observing L_α emission.

spherical symmetry of ns-state wave functions). For most other targets, the radiation polarizations are larger.

This predominance of ns-state excitation has a direct bearing on what might be expected from a measurement of L_α emission resulting from H + Ne collisions. For $n \geq 3$, these ns states decay preferentially to the $2p$ state, resulting in cascade contributions to the total L_α emission. Because of the long radiative lifetimes of excited ns states (all $\tau_{ns} \geq 1.6 \times 10^{-7}$ sec), the L_α signal from such cascade processes should depend on the distance into the target cell where the signal is observed, just as for the case of H_α and H_β emission from $ns \rightarrow 2p$ transitions. Indeed, it is this very fact which has been used here to obtain an absolute calibration of the detector used to study L_α emission from H + Ne collisions, as will be described in Sec. IV.

III. THE L_α DETECTOR

While the L_α detector took on several configurations during the course of these measurements, a typical configuration is shown in Fig. 3. Photons produced by H + Ne collisions entered the detector through a small square (or rectangular) aperture and were rendered into a parallel beam by the LiF lens. They then traversed an interference filter (with a 15-nm FWHM bandpass and peak transmission at about 124 nm) and an O_2 gas-cell filter (described below), and impinged on the photocathode of a solar-blind photomultiplier through its MgF_2 window. The photocathode was 11.5 cm from the H-beam axis, and the electron beam was 4.3 cm from the 0.4 cm diam entrance aperture to the target cell.

For the L_α radiation polarization measurements, a LiF window was mounted at the Brewster angle in the position where the photomultiplier is shown in Fig. 3. The reflected intensities $I_{||}$ and $I_\perp$ were measured by rotating the window by 90° about the optical axis.

The photomultiplier was operated in a pulse-counting mode, its amplified output being shared by two counters gated on/off to correspond to the beam on/off cycles.[1] Because all known sources of background counts were continuous in time, subtraction of the counts accumulated

by the counters provided a measure of the L_α photons from the collisions being investigated.

The O_2 gas-cell filter consisted of two LiF windows separated by 1.00 cm. Cold-trapped O_2 gas flowed through the filter at a rate of about 3 cm^3/sec, the O_2 pressure in the cell being held at about 720 Torr for most measurements. The absorption of ultraviolet light by O_2 between 105 and 135 nm was first studied by Watanabe *et al.*,[7] who found that the absorption coefficient was large except at seven narrow wavelength "windows" centered at 110.8, 112.7, 114.3, 115.7, 116.7, 118.7, and 121.6 nm, this last window being very close to the L_α wavelength (121.57 nm). Numerous workers have followed the pioneering work of Fite and Brackmann[8] in using such filters for wavelength discrimination during L_α emission cross-section measurements.

The use of a photomultiplier with a MgF_2 window and an interference filter in conjunction with an O_2 gas filter in the present experiment effectively blocked transmissions through the four shorter-wavelength windows identified above. Transmissions through the 116.7 and 118.7 nm windows were also reduced significantly relative to that through the 121.6 nm window. Nevertheless, emissions other than L_α could pass through the three longer-wavelength windows, and each reaction studied had to be analyzed for possible contamination of the desired L_α signal. For H + Ne collisions, the O_2 filter was not even needed, for the Ne spectrum is free of lines from 96 to 256 nm, and the Ne^+ spectrum from 46 to 168 nm,[9] so the interference filter alone isolated L_α.[10] Thus, the properties of the O_2 filter could be studied using H + Ne collisions as a source of L_α.

A plot of the relative filter transmission as a function of O_2 pressure is shown in Fig. 4. The line curve was calculated from

$$S(P)=S_0 e^{-K_p(P/760)L}, \tag{1}$$

where $S(P)$ is the L_α signal at O_2-cell pressure P, S_0 is the signal at $P=0$, L is the cell length (1.00 cm), P is the O_2 pressure (in Torr), and K_p (in cm^{-1}) is the O_2 absorption coefficient fitted to $K_p=0.269+0.000478P$. This K_p agrees well with other data, for example, by Watanabe *et al.*[7] Thus a pure L_α signal should increase by a factor of 1.79 when O_2 at 720 Torr is removed from the filter in the experiment, with any measured difference in this factor indicating that detected radiations other than L_α may be a problem.

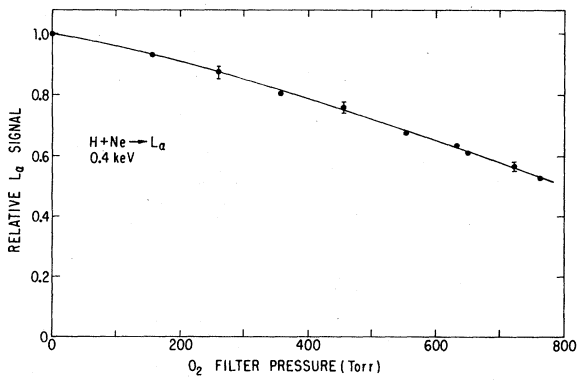

FIG. 4. Relative L_α signal versus O_2 filter pressure.

The H + Ne reaction also allowed an estimate to be made of the transmission of Doppler-shifted L_α by the O_2 filter. (While the detector's optical axis was at 90° to the H-beam axis, its viewing field accepted photons radiated at 90°±7° to the H-beam axis.) Comparison of the H-energy dependence of the L_α signals measured with and without O_2 in the filter showed that a small H-velocity-dependent factor (1.018±0.010, at $E=2.5$ keV) was needed to correct L_α signals measured with O_2 in the filter.

With the O_2-gas lines to the filter disconnected, the entire L_α detector shown in Fig. 3 could be moved parallel to the H-beam axis to observe L_α as a function of distance x into the target cell for $4 \leq x \leq 12$ cm. As indicated in Sec. II, the L_α signal from H + Ne collisions was found to increase with increasing x, the largest and most accurately measurable signal increases occurring for $1 \leq E \leq 2$ keV. How this signal increase with x was used to provide an absolute calibration of the L_α detector is described next.

IV. CALIBRATION OF THE L_α DETECTOR

The L_α signal from the cascade population of the $2p$ state of H in H + Ne collisions should be a function of distance x into the target cell. This can be written formally as[11]

$$s_{\rm cas}(x)=\epsilon \sum_{nl} Q'_{\rm em}(nl\rightarrow 2p)(1-e^{-x/v\tau_{nl}}), \tag{2}$$

$$=\epsilon Q'_{\rm cas}(2p)\left[\frac{\sum_{nl} Q'_{\rm em}(nl\rightarrow 2p)(1-e^{-x/v\tau_{nl}})}{\sum_{nl} Q'_{\rm em}(nl\rightarrow 2p)}\right]=S_{\rm cas}F(x), \tag{3}$$

where $S_{\rm cas}(x)$ is the normalized photon signal, the actual signal (in sec^{-1}) divided by the H flux (in sec^{-1}), the Ne density (in cm^{-3}), and the length of beam path (in cm) viewed by the detector, v is the H velocity (in cm/sec), τ_{nl} is the radiative lifetime (in sec) of an nl state of H which can populate the $2p$ state via $nl\rightarrow 2p$ cascade transitions, $Q'_{\rm em}(nl\rightarrow 2p)$ is the Balmer-line emission cross section (in cm^2) for the transition, $Q'_{\rm cas}(2p)$ is the sum of such cross

sections, i.e.,

$$Q'_{\rm cas}(2p)=\sum_{nl} Q'_{\rm em}(nl\rightarrow 2p) ,$$

ϵ is the total efficiency of the L_α detector, $S_{\rm cas}$ is the total normalized L_α signal from cascade processes (the value at infinite x), i.e., $S_{\rm cas}=\epsilon Q'_{\rm cas}(2p)$, and $F(x)$ is the quantity in the brackets in Eq. (3). Note that $F(x)$ is simply the fraction of the total normalized L_α signal from cascade from all nl states observed at distance x into the target cell.

In contrast, because of the very short radiative lifetime of the $2p$ state (1.6×10^{-9} sec), the normalized L_α signal from direct excitation to the $2p$ state should be effectively independent of x, i.e., $S_{2p}=\epsilon Q'_{\rm ex}(2p)$. Thus, if the total normalized L_α signal $S_m(x)$ vs x is measured and $F(x)$ calculated, S_{2p} and $S_{\rm cas}$ can be determined by fitting the $S_m(x)$ data to

$$S_m(x)=S_{2p}+S_{\rm cas}F(x) . \tag{4}$$

From this result, the fraction $f_{\rm cas}$ of the total L_α emission from cascade processes can be determined from

$$f_{\rm cas}=\frac{S_{\rm cas}}{S_{2p}+S_{\rm cas}}=\frac{Q'_{\rm cas}(2p)}{Q'_{\rm ex}(2p)+Q'_{\rm cas}(2p)} , \tag{5}$$

the second equality following from the fact that each normalized L_α signal must be in direct proportion to the corresponding emission cross section (i.e., $S=\epsilon Q'$). Thus, a knowledge of the various $Q'_{\rm em}(nl\rightarrow 2p)$ used to find $Q'_{\rm cas}(2p)$ and $F(x)$, and a measurement of $S_m(x)$, allows the cross section $Q'_{\rm ex}(2p)$ and the total L_α emission cross section

$$Q'_{\rm em}(L_\alpha)=Q'_{\rm em}(2p)+Q'_{\rm cas}(2p)$$

to be determined.

The data presented in Fig. 1 clearly show that for $1\leq E\leq 2$ keV, the $ns\rightarrow 2p$ transitions dominate the cascade population of the $2p$ state from the $n=3$ and 4 levels. In order to estimate how much $2p$-state population from higher-lying ns states might occur, the ratio of the cross sections for excitation to the $4s$ and $3s$ states was examined as a function of E. The result of this study is shown in Fig. 5, where the cross-section ratio $Q_{\rm ex}(4s)/Q_{\rm ex}(3s)$ has been multiplied by $(\frac{4}{3})^3$ for the comparison.[12] The parameter R plotted thus represents the departure of the cross-section ratio for ns-state excitation from the n^{-3} scaling law, which predicts that

$$Q_{\rm ex}(ns)\propto\frac{1}{n^3} , \tag{6}$$

as might be expected at high E. (Thus, if this law were to be followed here, the value of R would be unity.) As can be seen, R varies linearly with log E and extrapolates to zero at about the energy threshold for excited H production.

This rather surprising result led to examinations of R for the other H + target collisions investigated. While some of the data exhibited considerable scatter (because H_α and H_β emission from ns states is generally not so dominant as for Ne targets), for all reactions, the R

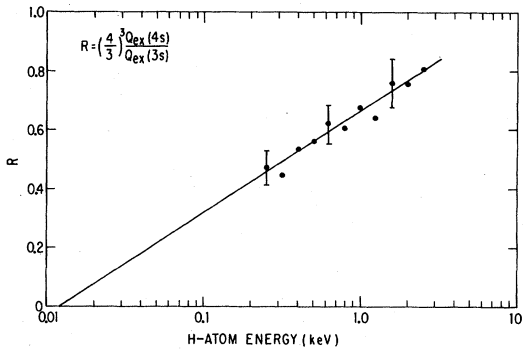

FIG. 5. Scaled excitation-cross-section ratio for $3s$ and $4s$ states populated in H + Ne collisions.

shown in Fig. 5 fitted the data to within measurement uncertainties, even though the excitation cross sections themselves exhibited differences in both magnitude and dependence on E.

It was assumed that the same R values would apply to excitation-cross-section ratios for higher-lying ns states. Thus, for example, it was predicted that $Q_{\rm ex}(5s)=R(\frac{4}{5})^3Q_{\rm ex}(4s)$ could be determined to within an estimated $\pm 50\%$ uncertainty for $1\leq E\leq 2$ keV, and that $Q_{\rm ex}(ns)$ could be determined for $n\geq 6$ to within an estimated $\pm 100\%$ uncertainty by successive step increases in n. While this assumption could not be tested for these higher-lying ns states, the cross section

$$Q_{\rm ex}(2s)=(1/R)(\tfrac{3}{2})^3Q_{\rm ex}(3s)$$

predicted from this model was in good agreement with the measured result (as will be shown in Sec. VII), lending confidence to use of the assumption for $n\geq 5$.

Figure 1 shows that for $1\leq E\leq 2$ keV, cascade population of the $2p$ state from $ns\rightarrow 2p$ transitions will be much larger than from $nd\rightarrow 2p$ transitions, which are only a part of the measured $Q_{\rm em}(np\rightarrow 2s+nd\rightarrow 2p)$. It was, however, desirable to have some estimate of the magnitude of cascade population of the $2p$ state from nd states. A study was thus made of the ratio of the excitation cross sections to the $4d$ and $3d$ states as a function of E for targets other than Ne ($nd\rightarrow 2p$ transitions being the source of larger fractions of the H_α and H_β emissions for the other reactions). The fit of the data to the R plotted in Fig. 5 was poor when an n^{-3} scaling law was used, generally giving R values only about 60% as large as those plotted.

On the hypothesis that the excitation cross sections should be strongly dependent on the small-radius part of the excited-state H wave function, the scaling law

$$Q_{\rm ex}(nl)\propto\frac{(n+l)!}{(n-l-1)!n^{2l+4}} \tag{7}$$

was investigated. The quantity on the right of Eq. (7) is simply the square of the coefficient of the leading term of the nl-state radial wave function. For ns states, it gives the familiar n^{-3} scaling law of Eq. (6). For np states,

$$Q_{\rm ex}(np)\propto\frac{(n+1)(n-1)}{n^5} , \tag{8}$$

and for nd states,

$$Q_{ex}(nd) \propto \frac{(n+2)(n+1)(n-1)(n-2)}{n^7} . \quad (9)$$

For excitation to the $3d$ and $4d$ states, application of Eq. (9) gives $R=1.665Q_{ex}(4d)/Q_{ex}(3d)$, if R is again defined as the departure of the cross-section ratio from this scaling-law prediction. With R determined in this way, the data for H impact on the various targets investigated generally did follow the dependence of R on E shown in Fig. 5 for $E>0.25$ keV. While the quality of the fit was not as good as for ns-state excitation (for example, giving R values 11% above and 30% below that plotted for H + He and H + Ar collisions, respectively, at $E=1.6$ keV), it was clearly better on average than that predicted by the n^{-3} scaling law and was used here for the estimates needed to evaluate nd-state excitation for H + Ne collisions in the same way that ns-state excitation was handled above.

The procedure used to analyze the L_α emission from H + Ne collisions for the detector calibration is summarized below. It was first assumed that the measured $Q'_{em}(np\rightarrow 2s+nd\rightarrow 2p)$ for $n=3$ and 4, similar to the $Q_{em}(np\rightarrow 2s+nd\rightarrow 2p)$ shown in Fig. 1 but not corrected for polarization, resulted entirely from $nd\rightarrow 2p$ transitions. These $Q'_{em}(nd\rightarrow 2p)$ were then used to estimate $Q'_{ex}(nd)$ for $n=3$ and 4, which were used together with the measured $Q'_{ex}(ns)$, the scaling laws from Eqs. (6) and (9), and the R from Fig. 5, to give a set of $Q'_{em}(nl\rightarrow 2p)$ for all $n\geq 3$. $Q'_{cas}(2p)$ and $F(x)$ were calculated, and measured values of $S_m(x)$ were used in Eqs. (4) and (5) to find $Q'_{ex}(2p)$. Assuming the scaling law in Eq. (8) for np-state excitation was valid (it could not be tested here), and again taking R from Fig. 5, $Q'_{ex}(np)$ were estimated from this $Q'_{ex}(2p)$. This allowed $Q'_{em}(np\rightarrow 2s)$ for $n=3$ and 4 to be determined, and these results were subtracted from the measured $Q'_{em}(np\rightarrow 2s+nd\rightarrow 2p)$ to obtain new values for $Q'_{em}(nd\rightarrow 2p)$. The entire process was then iterated until a reasonable convergence was obtained. The uncertainties assigned to the $Q'_{em}(nd\rightarrow 2p)$ resulting from the analysis were estimated to be ±100% of their determined values.

Three sets of measured $S_m(x)$ data at $E=1.6$ keV were used for the calibration. One set is shown in Fig. 6, along with the least-squares fit to the measured results. The values of S_{2p} and S_{cas} obtained from the fit and their uncertainties are indicated. A value of $f_{cas}=0.388\pm 0.6\%$ resulted from these data, the other sets of $S_m(x)$ data giving f_{cas} values of $0.389\pm 0.8\%$ and $0.389\pm 0.7\%$. The agreement among these values is very good, even though the data were taken at different times over the course of these studies, and with different L_α-detector configurations.[10]

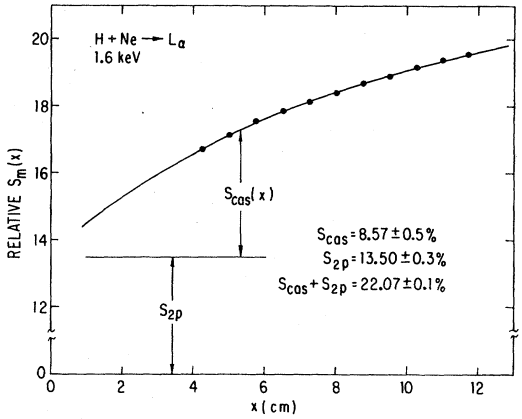

FIG. 6. Relative L_α signal $S_m(x)$ versus distance into target cell.

A summary of $Q'_{em}(nl\rightarrow 2p)$ and their estimated uncertainties for $E=1.6$ keV is presented in Table I, together with the fractions of the total cascade population of the $2p$ state resulting from the various transitions. As can be seen, the $3s\rightarrow 2p$ and $4s\rightarrow 2p$ transitions amount to about 90% of the total. The uncertainty assigned to the total $Q'_{cas}(2p)$ represents a direct sum of the individual uncertainties in the various $Q'_{em}(nl\rightarrow 2p)$ judged to be correlated, and a quadrature combination of those judged to be uncorrelated.

Using these results, the L_α emission cross sections for H + Ne collisions at 90° to the H-beam axis at $E=1.6$ keV were found to be the following: $Q'_{cas}(2p)=1.70\times 10^{-17}$ cm^2 ±13.7%, $Q'_{ex}(2p)=2.68\times 10^{-17}$ cm^2 ±14.0%, $Q'_{em}(L_\alpha)=4.38\times 10^{-17}$ cm^2 ±13.9%, and $Q'_{std}(L_\alpha)=3.32\times 10^{-17}$ cm^2 ±13.9%. This last cross section (the "measured" value at $x=4.3$ cm into the target cell) served as a detector-calibration standard on a daily basis to place other measurements on an absolute scale, i.e., to find the detector-efficiency calibration constant

TABLE I. Cascade cross sections.

Transition $nl\rightarrow 2p$	$Q'_{em}(nl\rightarrow 2p)$ (10^{-17} cm^2)	$Q'_{em}(nl\rightarrow 2p)$ Uncertainty	Fraction of total cascade
$3s\rightarrow 2p$	1.292[c]	±13.5%[c]	0.759
$4s\rightarrow 2p$	0.233[c]	±14.3%[c]	0.137
$5s\rightarrow 2p$	0.067	±50%	0.040
$ns\rightarrow 2p$[a]	0.045	±100%	0.026
$3d\rightarrow 2p$	0.041	±100%	0.024
$4d\rightarrow 2p$	0.013	±100%	0.008
$nd\rightarrow 2p$[b]	0.010	±100%	0.006
$Q'_{cas}(2p)$	1.701	±13.7%[d]	1.000

[a]Sum for $n\geq 6$.
[b]Sum for $n\geq 5$.
[c]Measured values from Fig. 1.
[d]See the text.

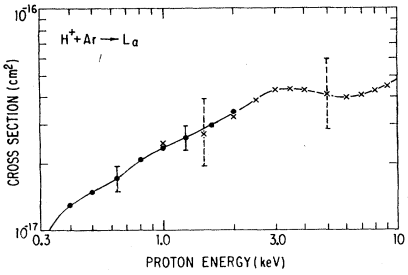

FIG. 7. L_α emission cross sections for $H^+ + Ar$ collisions. The data are from: ●, present results; ×, Pretzer *et al.* (Ref. 13).

$\epsilon = S_m$ (at $x = 4.3$ cm)$/Q'_{\rm std}(L_\alpha)$ as needed.

In order to investigate whether the L_α-detector calibration exhibited any dependence on E, $S_m(x)$ data were also measured for $E = 1.0$, 1.25, and 2.0 keV, and analyses like that described above were made. If the relative value of ϵ is set to 1.000 at $E = 1.6$ keV, the relative values at these other H energies were measured to be 1.003, 1.000, and 0.996, respectively. Considering that all relative ϵ values cited are uncertain by more than ±2.8% from the measurements alone, to say nothing about the dependence of the calculated $Q'_{\rm cas}(2p)$ and $f_{\rm cas}$ on E, this agreement was very satisfactory.

To compare this L_α-detector calibration with other work, the L_α emission cross section for $H^+ + Ar$ collisions was measured at 90° to the beam axis and at $x = 4.3$ cm into the target cell. The results are compared with those of Pretzer *et al.*[13] in Fig. 7. The agreement is well within the indicated uncertainties, a particularly satisfying result because this $H^+ + Ar \rightarrow L_\alpha$ reaction has been used as a standard by numerous workers to calibrate absolutely their own L_α detectors (for example, by Birely and McNeal,[14] whose results for L_α emission from H + Ne collisions will be shown later).

Another reaction frequently used as a standard for cross section measurements is $e^- + H_2 \rightarrow L_\alpha$. Fite and Brackmann[8] recognized early in their studies of this reaction that their photon detector (using an O_2-gas filter and an I_2-vapor photon counter, both with LiF windows, and calibrated absolutely by comparing L_α emission from $e^- + H$ collisions with Born-approximation calculations), could detect molecular H_2 emissions in addition to L_α. They thus measured only the cross section for countable ultraviolet (cuv) emission, reporting $Q'_{\rm em}(\text{cuv}) = 1.39 \times 10^{-17}$ cm^2 for 100 eV electrons. This value was subsequently revised to $Q_{\rm em}(\text{cuv}) = 1.48 \times 10^{-17}$ cm^2 ±3.6% by Kauppila *et al.*[15] Carrière and de Heer[16] studied the transmission of an O_2 filter by H_2 emissions (belonging to the Werner and Lyman bands), and estimated that about 80% of this cuv emission from $e^- + H_2$ collisions was L_α. Values of $Q_{\rm em}(L_\alpha)$ near 1.2×10^{-17} cm^2 have thus been adopted by most workers for detector calibrations.

It was thus with some surprise that the $Q_{\rm em}(\text{cuv})$ obtained here was found to be 8.49×10^{-18} cm^2 ±14.6% for 100 eV electrons.[17] Furthermore, it was estimated that between about 5% and 25% of the observed cuv signal was still coming from H_2 emissions.[18] Using the L_α emission fraction of 85±10% gives $Q_{\rm em}(L_\alpha)$ $= 7.22 \times 10^{-18}$ cm^2 ±18.8%. While this value agrees within uncertainties with the value 8.2×10^{-18} cm^2 ±15% recently determined by Shemansky *et al.*,[19] it is only about 60% of the generally adopted result cited above. If the present $Q_{\rm em}(L_\alpha)$ and the $Q_{\rm em}$ (cuv) of Kauppila *et al.*[15] are accepted, it appears that only about 50% of the cuv emission observed in the older studies was L_α, and that cross-section data obtained using $Q_{\rm em}(L_\alpha)$ as a calibration standard will require downward revision.

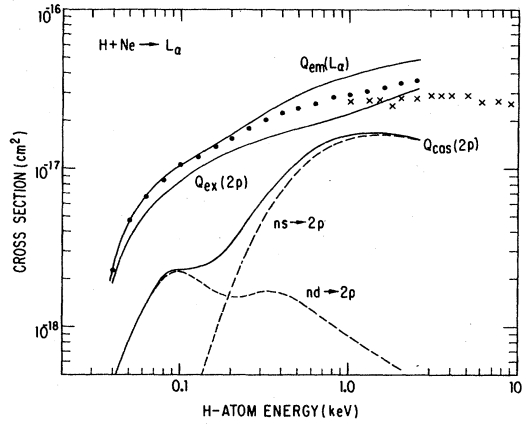

FIG. 8. L_α emission cross sections for H + Ne collisions. The data points are from: ●, present results for $Q_m(L_\alpha)$; ×, Birely and McNeal (Ref. 14). See the text for definitions of other cross sections shown.

V. L_α EMISSION CROSS SECTIONS

The L_α emission cross section for H + Ne collisions $Q_m(L_\alpha)$, measured at a distance of $x = 4.3$ cm into the target cell, is shown by the data points plotted in Fig. 8. The cross-section values have been placed on an absolute scale using the $Q'_{\rm std}(L_\alpha)$ discussed in Sec. IV, and have been adjusted to account for the measured L_α polarization at $x = 4.3$ cm shown in Fig. 9. The values plotted are uncertain by ±14.5% for $E \geq 0.1$ keV, the uncertainty increasing to about ±20% at 0.04 keV. The data of Birely and McNeal[14] are shown for comparison. The agreement is not highly satisfactory, but the two sets of data are within mutual uncertainties where they overlap.

The other cross sections shown in Fig. 8 were determined from

$$Q_{\rm ex}(2p) = Q_m(L_\alpha) - F(4.3) Q_{\rm cas}(2p) \qquad (10)$$

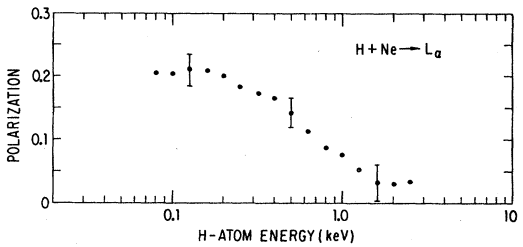

FIG. 9. Polarization of L_α radiation from H + Ne collisions.

and

$$Q_{em}(L_\alpha)=Q_{ex}(2p)+Q_{cas}(2p)\ . \tag{11}$$

In these expressions, $Q_{cas}(2p)$ is the cross section for the cascade population of the $2p$ state from $nl\rightarrow 2p$ transitions, determined from the H_α and H_β emission cross sections shown in Fig. 1 and the procedures discussed in Sec. IV for scaling the cascade cross sections from $n\geq 5$ levels. $F(4.3)$ is the fraction of this cascade cross section which results in observable L_α emission at $x=4.3$ cm into the target cell. $Q_{ex}(2p)$ is the cross section for direct excitation to the $2p$ state, and $Q_{em}(L_\alpha)$ is that for total L_α emission. The uncertainties in $Q_{em}(L_\alpha)$, $Q_{ex}(2p)$, and $Q_{cas}(2p)$ are close to those cited above for $Q_m(L_\alpha)$.

The short-dashed curves in Fig. 8 show the contributions made to $Q_{cas}(2p)$ by $ns\rightarrow 2p$ and $nd\rightarrow 2p$ transitions for all $n\geq 3$. The $ns\rightarrow 2p$ contribution for $E\geq 0.2$ keV, and the $nd\rightarrow 2p$ contribution for $E\leq 0.2$ keV, again have uncertainties similar to those cited above. However, for $E>0.2$ keV, the uncertainty in the $nd\rightarrow 2p$ contribution increases rapidly and is about $\pm 100\%$ of the contribution value for $E\geq 1$ keV. This is because of the approximate procedures used to find the separate $np\rightarrow 2s$ and $nd\rightarrow 2p$ contributions to the measured $Q_{em}(np\rightarrow 2s+nd\rightarrow 2p)$ shown in Fig. 1, for $n=3$ and 4 (see Sec. IV). The results of this separation are shown by the short-dashed curves in Fig. 1. At low E, where the predicted $np\rightarrow 2s$ contribution is very small, its large uncertainty has little influence on the $nd\rightarrow 2p$ contribution. However, where the contributions have similar values, both are highly uncertain.

Note that $Q_m(L_\alpha)$ and $Q_{em}(L_\alpha)$ are close in magnitude for $E\leq 0.2$ keV. This is as it should be, for the bulk of the L_α here results from $Q_{ex}(2p)$, and what cascade population of the $2p$ state is present is dominated by $nd\rightarrow 2p$ transitions, the nd states having fairly short radiative lifetimes. In contrast, $Q_m(L_\alpha)$ and $Q_{ex}(2p)$ are approaching similar values at the higher E, most of the cascade here being from long-lived ns states, the fraction of which show up as L_α emission at $x=4.3$ cm being small (e.g., ~ 0.3 at 2.5 keV).

VI. 2s-STATE EXCITATION CROSS SECTION

L_α emission from H + Ne collisions was also observed when the interaction region contained an electric field parallel to the H-beam axis. The electric field was produced by applying potentials V_f and V_b to the center two electrodes shown in Fig. 10 (separated by 3.14 cm along the beam axis and centered at the distance $x=4.3$ cm into the target cell). With this arrangement, it was necessary to examine the L_α signal versus the electric-field magnitude to determine if the signal was "saturated" so that L_α from only those H atoms excited in the detector's viewing field was being observed.

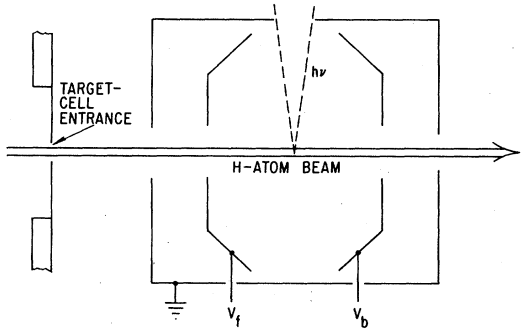

FIG. 10. Apparatus for producing an electric field in a target cell.

Electric fields of the same magnitude could be generated by any of the combinations of potentials: (a), $V_f=0$ and $V_b=\pm 2W$; (b), $V_f=\pm W$ and $V_b=\mp W$; or (c), $V_f=\pm 2W$ and $V_b=0$. In general, combination (a) required larger W to achieve L_α-signal saturation, because with $V_f=0$ there was no electric field between the first two electrodes (separated by about 1 cm) shown in Fig. 10. An electric field there served to prequench $2s$ atoms excited earlier along the H-beam path. The W required to achieve L_α-signal saturation for the various potential combinations was consistent with calculations made using the $2s$-state lifetime as a function of electric-field magnitude.[20] Potential combination (b) was finally adopted because of the smaller absolute values of V_f and V_b needed for any given electric field magnitude. However, for $W=1100$ V, giving the 700 V/cm electric field used for most measurements, the measured L_α signal and polarization were independent of the potential combination used.

It should also be noted that the various potential combinations discussed above gave electric fields both parallel and antiparallel to the H-beam axis. Although all data were taken with both electric-field directions, no measurable difference in either the L_α-signal magnitude or the radiation polarization was ever observed.

The measured L_α emission cross section for H + Ne collisions in a 700 V/cm electric field, $Q_m(L_\alpha)$, is shown by the data points in Fig. 11. The cross-section values have been adjusted to account for the polarization of the emitted radiation shown in Fig. 12. The average uncertainty of the plotted data is $\pm 15.3\%$.

The other L_α emission cross sections shown in Fig. 11 are related by

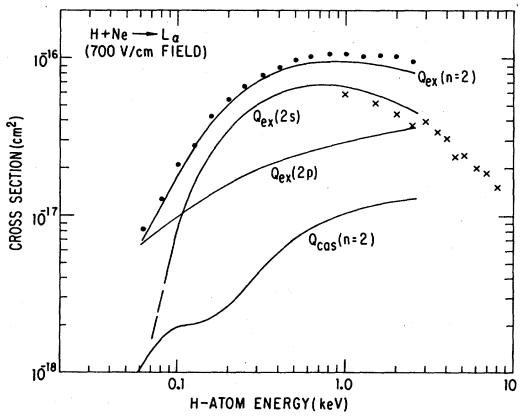

FIG. 11. L_α emission cross sections for H + Ne collisions in a 700 V/cm electric field. The data points are from: ●, present results for $Q_m(L_\alpha)$; ×, Birely and McNeal (Ref. 14). See the text for definitions of other cross sections shown.

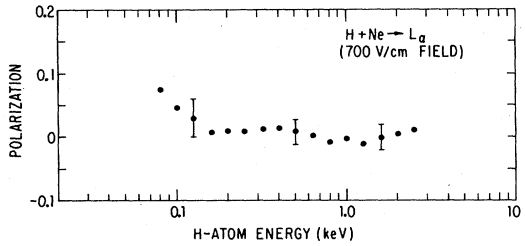

FIG. 12. Polarization of L_α radiation from H + Ne collisions in a 700 V/cm electric field.

$$Q_{ex}(n=2)=Q_m(L_\alpha)-Q_{cas}(n=2)\ , \tag{12}$$

$$=Q_{ex}(2s)+Q_{ex}(2p)\ . \tag{13}$$

Here, $Q_{ex}(n=2)$ is the cross section for excitation to the $n=2$ level of H, and $Q_{cas}(n=2)$ is the cross section for the cascade population of the $n=2$ level from all $n\geq 3$ levels. $Q_{ex}(2s)$ is the cross section for excitation to the $2s$ state, and $Q_{ex}(2p)$ is again that for excitation to the $2p$ state taken from Fig. 8, and assumed to remain unchanged by application of the electric field. It was assumed also that the radiative lifetimes of all excited states were sufficiently short in the 700 V/cm electric field that the L_α signals observed from all processes would be independent of distance x into the target cell;[21] hence $Q_m(L_\alpha)=Q_{em}(L_\alpha)$.

Unfortunately, $Q_{cas}(n=2)$ could not be determined here to high accuracy. While the cross sections for excitation to all nl states were estimated during the L_α-detector-calibration analysis discussed in Sec. IV, how the various m_l substates shared the nl-state populations could not be uniquely determined. In addition, only for the $n=3$ level were calculations available describing the branching ratios for nlm_l-substate decay to the $n=2$ level in a 700 V/cm electric field. These calculations, made by Rouze *et al.*,[22] are summarized in Table II.

The $Q_{cas}(n=2)$ shown in Fig. 11 was calculated using two approximations. First, it was assumed that the m_l substates of any given nl state were equally populated. Second, it was assumed that the branching ratios for decay of all nlm_l substates were the same as those for the $n=3$ level given in Table II.[23] Fortunately, the resulting $Q_{cas}(n=2)$, which must be considered uncertain by about $\pm 40\%$, is small compared to $Q_m(L_\alpha)$, so that the $Q_{ex}(n=2)$ determined from Eq. (12) is uncertain by only about $\pm 18\%$. This leads to an uncertainty in $Q_{ex}(2s)$ of about $\pm 30\%$ for $E\geq 0.16$ keV.

The $Q_{ex}(2s)$ determined by the above procedure may be compared with the measured values of Birely and McNeal[14] in Fig. 11. As can be seen, the present results are larger by about the same amount as shown in Fig. 8 for comparison of the L_α emission cross section.

VII. DISCUSSION OF THE RESULTS

One of the interesting features of the data reported here for H-atom excitation in low-energy H + Ne collisions is the reduced importance of interactions leading to *np*- and *nd*-state populations for H-atom energies in the 1 keV region. Figure 1 shows that for the $n=3$ and 4 levels, the *ns* states are much more heavily populated than other *nl* states. For no other target, including the other rare-gas atoms, or the N_2, O_2, and H_2 molecules,[1–3,6] has *ns*-state excitation been so dominant. It is not that $Q_{ex}(ns)$ is so large for Ne targets, but rather that $Q_{ex}(nl)$ for the other states are unusually small. Figure 11 shows that $Q_{ex}(2p)$ is also less than $Q_{ex}(2s)$ in this range of E, a result also unique to Ne targets. Indeed, even for He targets, the cross sections for *np*- and *nd*-state excitation are several times larger than those for Ne (even though the *ns*-state excitation cross sections for He are only about 25% as large as those for Ne).

While this diminished importance of *np*- and *nd*-state excitation in H + Ne collisions is not understood, it has provided an opportunity to examine *ns*-state excitation in detail (in addition to providing a new L_α-detector calibration). It was noted earlier[6] that the ratio of the $4s$- to $3s$-state excitation cross sections was close to the prediction of an n^{-3} scaling law for all rare-gas-atom targets. This has now been quantified, as shown by the data in Fig. 5, where the parameter R has been defined by the departure of this cross-section ratio from the n^{-3} law prediction. As noted in Sec. IV, a similar plot (although with increased data scatter) of this cross-section ratio for all other targets investigated yields the same dependence of R on E.

It was also noted in Sec. IV that if the scaling laws for *np*- and *nd*-state excitation given by Eqs. (8) and (9) are used, and R is again defined as the departure of the $Q_{ex}(4l)/Q_{ex}(3l)$ ratio from the scaling-law predictions, a generally similar dependence of R on E is consistent with the data for targets other than Ne. Analyses of the H_α emissions from decay of the $3s$, $3p$, and $3d$ states like that

TABLE II. Branching ratios for $n=3$ to $n=2$ transitions in a 700 V/cm electric field [data are from Rouze *et al.* (Ref. 22)].

Upper level substrate	Branching ratio to $n=2$ level
$3s_0$	0.416
$3p_0$	0.263
$3p_{\pm 1}$	0.341
$3d_0$	0.622
$3d_{\pm 1}$	0.372
$3d_{\pm 2}$	0.982

TABLE III. Ratio of measured to predicted $Q_{ex}(2s)$.

E (keV)	Measured $Q_{ex}(2s)$ / Predicted $Q_{ex}(2s)$
2.50	0.93
2.00	0.99
1.60	1.00
1.25	1.00
1.00	1.07
0.80	1.11
0.63	1.14
0.50	1.30

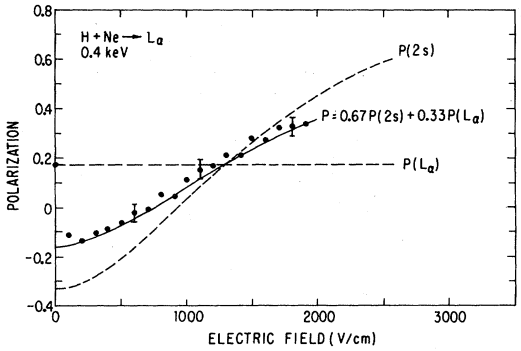

FIG. 13. Polarization of L_α radiation from H + Ne collisions as a function of electric field.

discussed here for Ne targets have now been completed. If it is assumed that the total H_α emission from decay of these states has been properly partitioned, the parameter R and the scaling laws assumed can be used to predict the total H_β emission from the various collisions as a function of E. The ratios of these predicted values to the measured results, when averaged over the data from $0.25 \leq E \leq 2.5$ keV, are the following: 0.90 for He; 1.07 for Ar, N_2, and O_2; 1.09 for Kr; and 1.31 for Xe.[24] Considering the large differences among these targets in the magnitudes and H-energy dependences of these cross sections, the quality of these predictions is remarkable.

In order to examine whether the parameter R was unique to the $n=3$ and 4 levels of H, the cross section for excitation to the $2s$ state was predicted from

$$Q_{ex}(2s)=(1/R)(\tfrac{3}{2})^3 Q_{ex}(3s) ,$$

and is compared with the data (from Fig. 11) in Table III for $E \geq 0.5$ keV. While there is some trend in the measured to predicted cross-section ratio with E, it is again remarkable that this simple model could make predictions of this quality. (While the data for $2s$-state excitation for the other rare-gas atom and molecular targets have not yet been finally analyzed, preliminary considerations suggest that generally similar results will be obtained.)

It is clear that the parameter R and the scaling laws used in the analysis described in this paper apply to many different H-atom-excitation processes. It would be difficult to conclude that their application is only accidentally valid.

The high positive polarization of the L_α radiation resulting from H + Ne collisions for $E \leq 0.5$ keV (see Fig. 9) suggests that most of the $2p$-state-excited H atoms are here being produced in the $m_l=0$ substate.[25] (This is another example of the uniqueness of Ne as a target, for L_α radiation from other H + target collisions is less polarized.) The rapid decrease of the polarization at higher E may be due in part to the importance of cascade population of the $2p$ state from higher ns states, which should give unpolarized L_α.

The polarization of the L_α radiation from H + Ne collisions in a 700 V/cm electric field (see Fig. 12) is near zero for $E \geq 0.2$ keV (although it increases at low E where an increasing amount of the L_α comes from $2p$-state excitation). This fact, however, is an artifact of using an electric field of 700 V/cm magnitude. While not part of the main theme of this paper, the polarization of L_α from H + Ne collisions was studied as a function of electric-field magnitude. The result of this study is shown in Fig. 13.

For $E=0.4$ keV with the electric field on, about 67% of the total observed L_α results from excitation to the $2s$ state. The polarization of L_α from electric-field quenching (i.e., $2s$- and $2p$-state mixing) of this state was calculated by Crandall[26] as a function of electric-field magnitude, and is shown as the short-dashed curve labeled $P(2s)$ in Fig. 13. The short-dashed curve labeled $P(L_\alpha)$ is the L_α polarization measured here with no electric field (which was assumed to remain unchanged when the electric field was applied[27]). Thus for an electric field above about 200 V/cm, the curve labeled $P=0.67P(2s)+0.33P(L_\alpha)$ is approximately what would be expected from the indicated relative weighting of the other curves, and may be compared with the measured total L_α polarization as a function of electric field shown by the data points. As can be seen, the agreement is generally satisfactory, supporting the validity of both the measured and calculated results.

ACKNOWLEDGMENTS

The authors thank R. C. Amme and P. S. Ormsby for their contributions to this research, and Shemansky *et al.*[19] and Rouze *et al.*[22] for permission to cite their data prior to publication. This work has been supported by the Aeronomy Program, Division of Atmospheric Sciences, National Science Foundation.

[1]B. Van Zyl, H. Neumann, H. L. Rothwell, Jr., and R. C. Amme, Phys. Rev. A **21**, 716 (1980).

[2]B. Van Zyl, M. W. Gealy, and H. Neumann, Phys. Rev. A **28**, 176 (1983).

[3]B. Van Zyl and H. Neumann, J. Geophys. Res. **85**, 6006 (1980).

[4]B. Van Zyl, N. G. Utterback, and R. C. Amme, Rev. Sci. Instrum. **47**, 814 (1976).

[5]B. Van Zyl, Rev. Sci. Instrum. **47**, 1214 (1976).

[6]H_α and H_β emission cross sections and radiation polarizations for H impact on all rare-gas atoms were presented at: B. Van Zyl, M. W. Gealy, H. Neumann, and R. C. Amme, in *Proceedings of the Thirteenth International Conference on the Physics of Electronic and Atomic Collisions*, edited by J. Eicher, W. Fritsch, I. V. Hertel, N. Stolterfoht, and U. Wille (Freie Universität Berlin, Berlin, 1983), p. 335.

[7]K. Watanabe, E. C. Y. Inn, and M. Zelikoff, J. Chem. Phys. **21**, 1026 (1953).

[8]W. L. Fite and R. T. Brackmann, Phys. Rev. **112**, 1151 (1958).

[9]A. R. Striganov and N. S. Sventitskii, *Tables of Spectral Lines of Neutral and Ionized Atoms* (IFI/Plenum, New York, 1968).

[10]In fact, some data for H + Ne collisions were taken without including even the interference filter, using the rapid decrease in the photocathode quantum efficiency above 150 nm as the only wavelength discrimination.

[11]These expressions are used for purposes of exemplification only. More complicated expressions, including the effect of the pressure gradient near the target-cell entrance and the pressure in the vacuum tank prior to the target cell, were used for data analysis. These expressions also assume that the $2p$-state lifetime is zero, a good approximation here.

[12]These $Q_{ex}(ns)$ were assumed to be given by the measured $Q_{em}(ns \rightarrow 2p)$ divided by the $ns \rightarrow 2p$ branching ratios, i.e., cascade to these ns states from still higher-lying np states was neglected. This is a good approximation because these high-lying np states decay very preferentially to the $1s$ and $2s$ states. Note also that for all ns states, cross sections $Q = Q'$, because decay of these states must give unpolarized radiation.

[13]D. Pretzer, B. Van Zyl, and R. Geballe, in *Atomic Collision Processes,* edited by M. R. C. McDowell (North-Holland, Amsterdam, 1964), p. 618.

[14]J. H. Birely and R. J. McNeal, Phys. Rev. A **5**, 257 (1972).

[15]W. E. Kauppila, P. J. O. Teubner, W. L. Fite, and R. J. Girnius, J. Chem. Phys. **55**, 1670 (1971).

[16]J. D. Carrière, and F. J. de Heer, J. Chem. Phys. **56**, 2993 (1972).

[17]This value was obtained from the measured $Q'_{em}(\text{cuv}) = 8.62 \times 10^{-18}$ cm^2 using the measured polarization of cuv emission from 100 eV electrons on H_2 of $P = 0.045$ from W. R. Ott, W. E. Kauppila, and W. L. Fite, Phys. Rev. A **1**, 1089 (1970).

[18]This estimate was based on numerous considerations including the relative photon-detector efficiency versus wavelength, the relative transmission of H_2 emissions through the O_2-filter wavelength windows estimated by Carrière and de Heer (Ref. 16), private communication with D. E. Shemansky who has examined this problem in some detail, and a variety of experimental tests of the data. For example, the measured cuv signal increased by about 450% when O_2 at 720 Torr was evacuated from the filter. However, for O_2-filter pressures above 500 Torr, the cuv signal exhibited the same dependence on pressure shown in Fig. 4 for pure L_α, suggesting that most of the cuv signal observed here was L_α.

[19]D. E. Shemansky, J. M. Ajello, and D. T. Hall, Astrophy. J. (to be published).

[20]G. Lüders, Z. Naturforsch. **5a**, 608 (1950).

[21]This should be a reasonable approximation, because all nl states become mixed in such a high electric field and assume the short radiative lifetimes of np states.

[22]N. Rouze, C. C. Havener, W. B. Westerveld, and J. S. Risley, private communication. The data tabulated ignore off-diagonal terms in the density matrix. These are expected to be small.

[23]This was estimated to be a better approximation than ignoring cascade from all $n \geq 4$. If cascade from $n \geq 4$ is ignored, the $Q_{cas}(n = 2)$ values decrease by about 25%.

[24]The value for Xe may be in error because of possible spectral contamination of the H_α by Xe radiations. H_2 was not included because of the unknown amount of target emission observed. The value for Ne would be 1.00, because it was fitted to the model.

[25]U. Fano and J. H. Macek, Rev. Mod. Phys. **45**, 553 (1973).

[26]D. H. Crandall, Ph.D. dissertation, University of Nebraska, 1970 (unpublished).

[27]This assumption is not totally correct because of the change in the cascade contribution to the L_α signal when the electric field is applied.